DOI: 10.64302/joshusc.v35n2.1432

COMPUTATIONAL SCREENING OF NUCLEOSIDES FROM *CORDYCEPS CICADAE* AS α-GLUCOSIDASE INHIBITORS FOR DIABETES

Nguyen Cong Kinh[1,2], Nguyen Dai Chau[1], Pham Van Vinh[1], Nguyen Vinh Phu[3], Phan Tu Quy[4], Tran Quang Huy[1], Nguyen Thi Thanh Hai[1], Nguyen Thi Ai Nhung[1,*]

[1]Faculty of Chemistry, University of Sciences, Hue University

[2] Faculty of Pharmacy, Duy Tan University

[3]Faculty of Basic Sciences, University of Medicine and Pharmacy, Hue University

[4]Department of Natural Sciences & Technology, Tay Nguyen University

*Email: ntanhung@hueuni.edu.vn

Received: 13/7/2026; Received in revised form: 4/8/2026; Accepted: 4/9/2026

ABSTRACT

α-glucosidase inhibition slows intestinal carbohydrate digestion and remains a practical strategy for controlling postprandial hyperglycemia in diabetes. Five nucleosides and nucleoside derivatives from *Cordyceps cicadae*, namely, N6-(2-hydroxyethyl)-adenosine (**C1**), thymidine (**C2**), uridine (**C3**), 2′-deoxyinosine (**C4**), and 2′-deoxyguanosine (**C5**) were evaluated against α-glucosidase (PDB ID: 3W37) by molecular docking, 100 ns molecular dynamics simulation, drug-likeness assessment, and ADMET prediction, as the reference inhibitor (**D**). Binding-site prescreening across four candidate sites determined the preferred docking position for each compound. Docking scores ranked **C3** (-12.0 kcal.mol^{-1}) > **C2** (-11.9 kcal.mol^{-1}) > **C4** (-11.6 kcal.mol^{-1}) > **C5** (-10.8 kcal.mol^{-1}) > **C1** (-10.0 kcal.mol^{-1}), with **C3** showing the most favorable predicted binding and twelve van der Waals interactions at Site 2. Backbone RMSD of the **C3-3W37** complex restabilized near 0.28 nm after a transient excursion at 60–80 ns, during which the three to four hydrogen bonds maintained over most of the trajectory briefly fell to one or two, while Rg and SASA remained consistent. All five compounds satisfied Lipinski's Rule of Five, and ADMET profiling indicated favorable pharmacokinetic profiles, with **C3** presenting the most acceptable predicted safety margins. Within the limits of these in silico predictions, **C3** emerges as a prioritized candidate for subsequent experimental evaluation.

Keywords: *Cordyceps cicadae*, α-glucosidase, 3W37, computational study.

1. INTRODUCTION

Diabetes mellitus is a chronic metabolic disorder and a major public health burden worldwide, with type 2 diabetes mellitus being the predominant form, characterized by impaired glucose regulation and sustained hyperglycemia [1]. Delaying intestinal carbohydrate digestion by inhibiting α-glucosidase, an enzyme involved in the final hydrolysis of oligosaccharides and disaccharides into absorbable glucose, is a practical approach to reduce postprandial glucose elevation [2]. Acarbose is a widely used commercial α-glucosidase inhibitor, but its clinical use is often accompanied by gastrointestinal side effects [3]. Therefore, the search for natural compounds from medicinal plants with α-amylase and α-glucosidase inhibitory activity remains important for developing alternatives to current commercial drugs.

The genus *Cordyceps* has long been studied as a source of medicinal fungi with diverse chemical constituents and pharmacological activities [4, 5]. Among these, nucleosides and nucleoside derivatives recur across species of the genus and have served as marker compounds in phytochemical and bioactivity studies of *Cordyceps* [4, 5]. This class has been associated with antioxidant, anti-inflammatory, immunomodulatory, antiviral, and antitumor activities reported for the genus [5, 6]. *Cordyceps cicadae (C. cicadae)* in particular is a documented source of multiple nucleosides [7, 8]. Five representative constituents were selected to span the principal nucleoside subclasses found in this species: uridine and thymidine as pyrimidine nucleosides, 2′-deoxyinosine and 2′-deoxyguanosine as purine deoxynucleosides, and N6-(2-hydroxyethyl)-adenosine as a modified adenosine derivative. This set spans both nucleosides and their derivatives, allowing their binding behaviour toward α-glucosidase to be compared across the group.

In silico methods can prioritize candidates prior to enzyme assays, particularly when experimental data on the target compounds are limited. Molecular docking was used to predict the binding modes of the selected compounds at the α-glucosidase active site and to identify the main protein-ligand interactions. Molecular dynamics simulation was then performed to assess the stability and dynamic behavior of the resulting complexes; RMSD (Root Mean Square Deviation), RMSF (Root Mean Square Fluctuation), Rg (radius of gyration), SASA (Solvent Accessible Surface Area), and hydrogen bond occupancy were tracked to monitor structural fluctuation, compactness, solvent exposure, and interaction persistence. Drug-likeness and ADMET predictions were further included to provide an early indication of physicochemical suitability, pharmacokinetic behavior, and toxicity-related risks. Accordingly, the present study evaluates the five *C. cicadae*-derived nucleosides and the nucleoside derivative against α-glucosidase by molecular docking, molecular dynamics simulation, drug-likeness assessment, and ADMET prediction, with acarbose as the reference inhibitor.

2. METHODS

2.1. Molecular docking simulation

Molecular docking was performed in MOE software version 2022.10 [9] to predict the binding energies and interaction modes between each ligand and the α-glucosidase enzyme, and to propose a putative inhibitory mechanism. The protein target was retrieved from a public repository, its binding site was defined by the residues within 4.5 Å of the co-crystallized ligand together with the key catalytic amino acids, and water molecules and non-essential polymer chains were removed before the pocket was reconstructed. Each ligand was drawn and converted to a 3D structure in ChemBioOffice 2018, then energy-minimized in SYBYL-X 1.1 using the conjugate gradient method (Gasteiger–Hückel charges; energy-change cutoff of 0.001 kcal.mol^{-1}; maximum 10,000 iterations), with five repeated runs and re-minimization to select the more stable conformers by steric energy. Docking retained up to 1,000 results per iteration and 200 per ligand fragmentation, with the favored pose taken as that of lowest docking score (DS). The protocol was validated by re-docking the co-crystallized ligand, considered reliable at a backbone RMSD below 2.0 Å. The predicted inhibition was then assessed from DS (kcal.mol^{-1}), RMSD (Å), and the number of ligand-protein interactions (H-donor, H-acceptor, H-π, …) and van der Waals interactions with bonding and steric complementarity examined through 2D interaction maps and 3D models.

2.2. Molecular dynamics simulation

The MD protocol was implemented in GROMACS 2023 with the CHARMM27 force field, with ligand parameters prepared in SwissParam. Each complex was centered in a cubic TIP3P water box, and Na^+ and Cl^- ions were introduced to neutralize the system. Energy minimization preceded equilibration, which was performed sequentially in the NVT and NPT ensembles at 300 K and 1 bar. The Verlet integrator and the LINCS constraint algorithm were applied throughout the simulations [10]. Convergence and stability were tracked via RMSD, RMSF, Rg, and SASA, and VMD was used to detect hydrogen bonds with a 3.5 Å donor–acceptor distance and a 120° angle cutoff.

2.3. Drug-likeness prediction

Physicochemical and pharmacokinetic properties were predicted with ADMETLab 3.0 (https://admetlab3.scbdd.com/). Molecular weight (MW), octanol–water partition coefficient (logP), hydrogen bond donors (HBD), and hydrogen bond acceptors (HBA) were evaluated against Lipinski's rule of five [11] namely (i) MW ≤ 500 Da, (ii) HBD ≤ 5, (iii) HBA ≤ 10, and (iv) logP < 5. Molecular polarizability (Å^3) was obtained separately by geometry-optimizing each structure in Chem3D and submitting the optimized geometry to the AlphaML web server (https://alphaml.materialscloud.io),

which predicts static polarizability from a machine-learning model trained on coupled-cluster reference data.

2.4. ADMET prediction

ADMET properties (Absorption, Distribution, Metabolism, Excretion, and Toxicity) were obtained from a web-based regressive model developed and maintained by the Molecular Modeling Group, Swiss Institute of Bioinformatics, i.e. SwissADME (http://www.swissadme.ch/). The theoretical interpretations of the output pharmacokinetic parameters were described by Pires et al. [12] and powered by the University of Melbourne and the University of Cambridge for public reference (http://biosig.unimelb.edu.au/pkcsm/).

3. RESULTS AND DISCUSSION

3.1. The input data of the compounds and proteins studied

The nucleoside derivative N6-(2-hydroxyethyl)-adenosine (**C1**) and four nucleosides (**C2–C5**) from *C. cicadae* [7, 8] were investigated. For comparison, acarbose, a commercial antidiabetic drug, was also used as a reference drug. Their structures and molecular formulas are shown in Figure 1 and Table 1. The crystal structure of α-glucosidase (PDB ID: 3W37, https://doi.org/10.2210/pdb3W37/pdb), shown in Figure 2. This structure is an α-glucosidase from *Beta vulgaris* rather than the human enzyme. Both belong to glycoside hydrolase family 31 (GH31) and have similar catalytic sites [13], and plant α-glucosidases have been used as structural models in in silico inhibitor-screening studies [14]. Therefore, protein 3W37 was used as the protein target for the docking and dynamics studies, and the results are presented as a prescreening step towards the human enzyme.

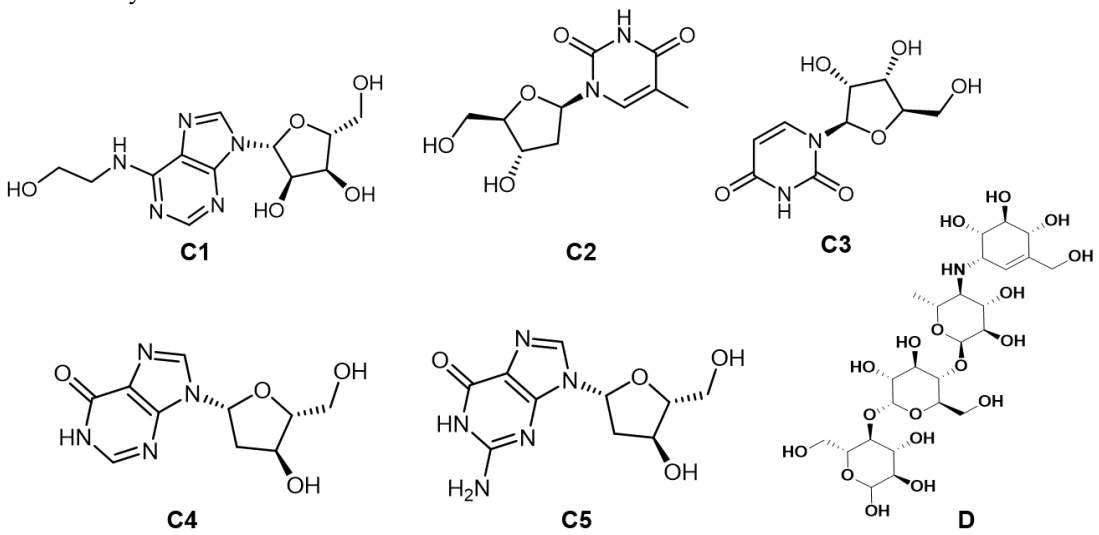


Figure 1. Chemical structures of the investigated compounds (**C1–C5**) and acarbose (**D**)

Table 1. Chemical identities of compounds **C1–C5** and the reference drug acarbose (**D**)

No.	Compound	Formula	Notation	Reference
1	N6-(2-hydroxyethyl)-adenosine	$C_{12}H_{17}N_5O_5$	**C1**	[7]
2	Thymidine	$C_{10}H_{14}N_2O_5$	**C2**	[8]
3	Uridine	$C_9H_{12}N_2O_6$	**C3**	[8]
4	2′-deoxyinosine	$C_{10}H_{12}N_4O_4$	**C4**	[8]
5	2′-deoxyguanosine	$C_{10}H_{13}N_5O_4$	**C5**	[8]
6	Acarbose	$C_{25}H_{43}NO_{18}$	**D**	

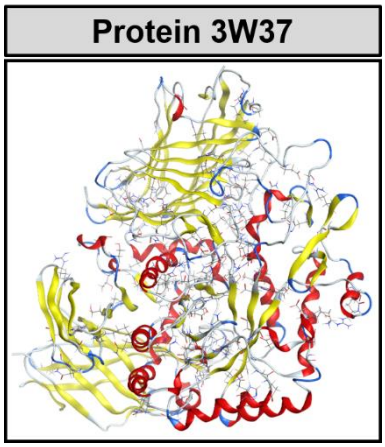


Figure 2. Crystal structure of α-glucosidase (PDB ID: 3W37) used as the protein target

3.2. Molecular docking analysis

The predicted binding affinity of **C1–C5** against α-glucosidase (3W37) was assessed from the docking score (DS, kcal.mol^{-1}), the RMSD (Å), and the intermolecular interactions, such as ligand-protein interaction (H-donor, H-acceptor, π-H, …) and van der Waals interaction formed with the binding-site residues, providing insight into the binding affinity and molecular recognition of the ligand–protein complexes.

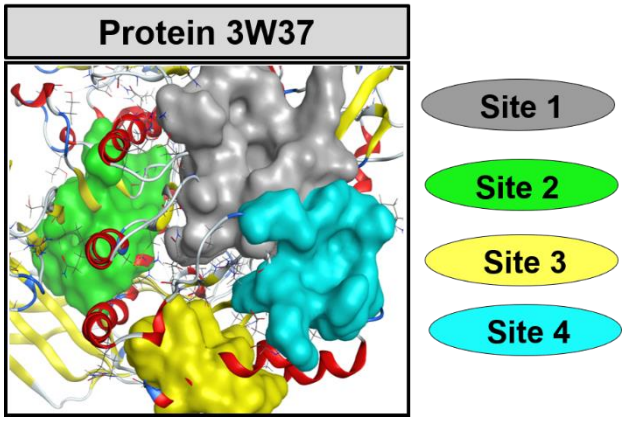


Figure 3. Quaternary structure of 3W37 with approachable sites by **C1–C5** and **D**: site 1 (gray), site 2 (green), site 3 (yellow), site 4 (cyan)

Table 2. The binding-site prescreening of compounds **C1**–**C5** and **D** of protein 3W37

Compound	Site 1		Site 2		Site 3		Site 4	
	E	**N**	**E**	**N**	**E**	**N**	**E**	**N**
C1	-8.9	1	-10.0*	2*	-8.7	1	-8.2	0
C2	-9.7	2	-10.0	3	-9.4	2	-11.9*	6*
C3	-10.9	3	-12.0*	6*	-9.8	2	-9.5	2
C4	-11.6*	4*	-9.6	2	-9.3	2	-8.6	1
C5	-8.8	1	-10.8*	3*	-8.5	1	-7.7	0
D	-12.1*	5*	-10.3	2	-10.0	2	-8.7	1

E: DS value (kcal.mol^{-1}); **N**: Number of ligand-protein interaction

The docking results describe the binding properties of each compound (**C1–C5**) relative to the *α*-glucosidase target (3W37), with the reference drug **D** included for comparison, using the DS and ligand–protein interaction profiles as indicators of binding favorability. The binding-site prescreening of compounds **C1**–C**5** and **D** against the four potential binding sites of 3W37 is summarized in Table 2 and Figure 3. The preferred sites were identified from the most negative DS values together with the highest number of interactions (N). Site 2 was the most frequently favored site, being suitable for compounds **C1**, **C3**, and **C5**, whereas Site 1 was preferred by compound **C4** and **D**, and Site 4 by compound **C2**. By contrast, Site 3 was not selected as the primary binding region for any of the investigated ligands. These findings agree with the binding-site characteristics in Table 3, which lists the size and amino acid residues at each surveyed position. In particular, Site 1 and Site 2 showed the two largest sizes among the four positions (64 and 37, respectively), supporting their identification as the preferred binding sites, while Site 3 displayed the smallest size (19), consistent with the absence of any ligand selecting it as the primary binding region. Specifically, Site 1 is the main catalytic site of 3W37 where inhibitors prevent substrate binding. Meanwhile, Site 2 serves as an accessory site where compound binding sterically prevents substrate access, thereby inhibiting substrate hydrolysis and enhancing overall enzyme inhibition [13].

Table 3. The binding-site characteristics of protein 3W37

Site	Size	Residues
1	64	Asp 232, Ile 233, Ala 234, Phe 236, Tyr 243, Trp 329, Asp 357, Ile 358, Ile 396, Trp 432, Trp 467, Asp 469, Met 470, Phe 476, Arg 552, Trp 565, Gly 567, Asp 568, Phe 601, Arg 624, His 626

2	37	Glu 301, Tyr 659, Thr 662, Leu 663, Asp 666, Arg 670, Arg 676, Gly 698, Arg 699, Gly 700, Asn 758, Ile 759, Val 760, Ala 761, Gly 791, Glu 792
3	19	Val 341, Asp 342, Tyr 344, Ala 345, Ile 349, Pro 350, Leu 351, Lys 385, Asn 389, Gln 391, Met 767, Thr768
4	23	Tyr 331, Arg 332, Ile 358, Asp 359, Met 361, Ala 363, Phe 364, Asp 370, His 373, Phe 374, Arg 629

Table 4. Molecular docking simulation results for ligands-**3W37** docking complexes

Ligand-protein complex			**Ligand-protein interactions**						**van der Waals interaction**
Name	**DS**	**RMSD**	**L**	**P**		**T**	**D**	**E**	
C1-3W37	-10.0	1.85	O	O	Asp 666	H-donor	3.05	-1.6	Asn 758, Tyr 659, Arg 676, Tyr 665, Gly 698, Gly 700, Arg 670, Ile 759, Leu 663, Gly 791, Arg 814, Leu 669, Glu 792
			O	N	Arg 699	H-acceptor	3.06	-2.1	
C2-3W37	-11.9	0.92	C	O	Asp 359	H-donor	3.44	-0.5	Phe 374, Asp 370, Arg 332, Arg 629, Ile 358, Asp 362, Phe 364
			O	O	Tyr 331	H-donor	2.86	-2.3	
			N	O	Met 361	H-donor	3.45	-1.3	
			O	C	Asp 359	H-acceptor	3.49	-0.5	
			O	N	Ala 363	H-acceptor	3.10	-0.9	
			C	5-ring	His 373	H-π	4.25	-1.8	
C3-3W37	-12.0	0.73	O	O	Glu 792	H-donor	2.93	-1.5	Gly 698, Arg 676, Arg 670, Asp 666, Thr 790, Leu 663, Asn 758, Glu 301, Ala 761, Thr 662, Tyr 665, Gly 791
			N	O	Ile 759	H-donor	2.88	-6.2	
			O	N	Arg 699	H-acceptor	3.10	-1.0	
			O	C	Val 760	H-acceptor	3.46	-0.7	
			6-ring	C	Tyr 659	π-H	3.80	-0.6	
			6-ring	C	Glu 792	π-H	4.28	-0.6	
C4-3W37	-11.6	1.40	O	O	Asp 568	H-donor	2.99	-1.1	Asp 232, Trp 329, Gly 567, Trp 432, Asp 469, Arg 552, Ile 396, Trp 565, Trp 467
			C	S	Met 470	H-donor	3.54	-0.7	
			O	O	Asp 357	H-donor	3.30	-1.1	
			C	6-ring	Phe 601	H-π	4.22	-0.5	
C5-3W37	-10.8	1.75	O	O	Glu 792	H-donor	3.06	-0.8	

			O	N	Glu 792	H-acceptor	3.19	-0.5	Arg 814, Gly 791, Thr 662, Tyr 659, Thr 790, Leu 663, Gly 700, Gly 698, Ile 759, Phe 816
			O	N	Arg 699	H-acceptor	3.18	-1.7	
D-3W37	-12.1	1.11	O	O	Asp 232	H-donor	3.07	-1.5	Ala 602, Ala 628, Glu 603, Trp 329, Phe 601, Asn 475, Ser 474, Met 470, Trp 432, Phe 230, Ala 234, Asp 568
			O	O	Asp 630	H-donor	2.92	-2.8	
			O	N	Lys 506	H-acceptor	3.16	-3.8	
			O	N	Lys 506	H-acceptor	2.99	-2.9	
			C	6-ring	Phe 476	H-π	4.57	-0.5	

DS: Docking score energy (kcal.mol^{-1}); **RMSD**: Root-mean-square deviation (Å); **L**: Ligand; **P**: Protein; **T**: Type; **D**: Distance (Å); **E**: Energy (kcal.mol^{-1})

Table 4 summarizes the molecular docking results for compounds **C1–C5** and the reference drug **D** (acarbose) against protein 3W37, and Figure 4 shows the corresponding 2D and 3D binding modes. The ligands engage the binding site mainly through their O, N, and C atoms together with aromatic rings, forming hydrogen bonds (H-donor and H-acceptor), H-π, and van der Waals interactions with the surrounding residues. All RMSD values fell below 2 Å, indicating that the predicted poses are reliable. The DS values of the studied compounds ranged from -10.0 to -12.0 kcal.mol^{-1}, compared with -12.1 kcal.mol^{-1} for **D**, indicating a predicted binding tendency comparable to that of the reference drug across the series. Ranked by DS, the predicted binding affinity decreased in the order **C3-3W37** (-12.0 kcal.mol^{-1}) > **C2-3W37** (-11.9 kcal.mol^{-1}) > **C4-3W37** (-11.6 kcal.mol^{-1}) > **C5-3W37** (-10.8 kcal.mol^{-1}) > **C1-3W37** (-10.0 kcal.mol^{-1}). Among them, **C3** showed the most favorable predicted binding. It is stabilized by six ligand–protein interactions (four H-donor and H-acceptor with Glu 792, Ile 759, Arg 699, and Val 760, and two π-H with Tyr 659 and Glu 792) and twelve van der Waals interactions, matching the twelve formed by **D**. **C3** and **C2** differ by only 0.1 kcal.mol^{-1} in DS, which is too small to separate them, but their interaction profiles differ. **C2** also forms six ligand-protein interactions, yet only seven van der Waals interactions. In addition, while data in Table 2 show that **C4** (-11.6 kcal.mol^{-1}) was closer to acarbose (-12.1 kcal.mol^{-1}) at Site 1, **C3** consistently formed multiple interactions across different sites; furthermore, detailed docking at their respective optimal sites (Table 4) showed that C3 established twelve van der Waals contacts at Site 2, compared to only seven for C4 at Site 1. Therefore, **C3** was carried forward as the most promising compound of the series, and because a 100 ns simulation is computationally demanding, it was the only compound simulated.

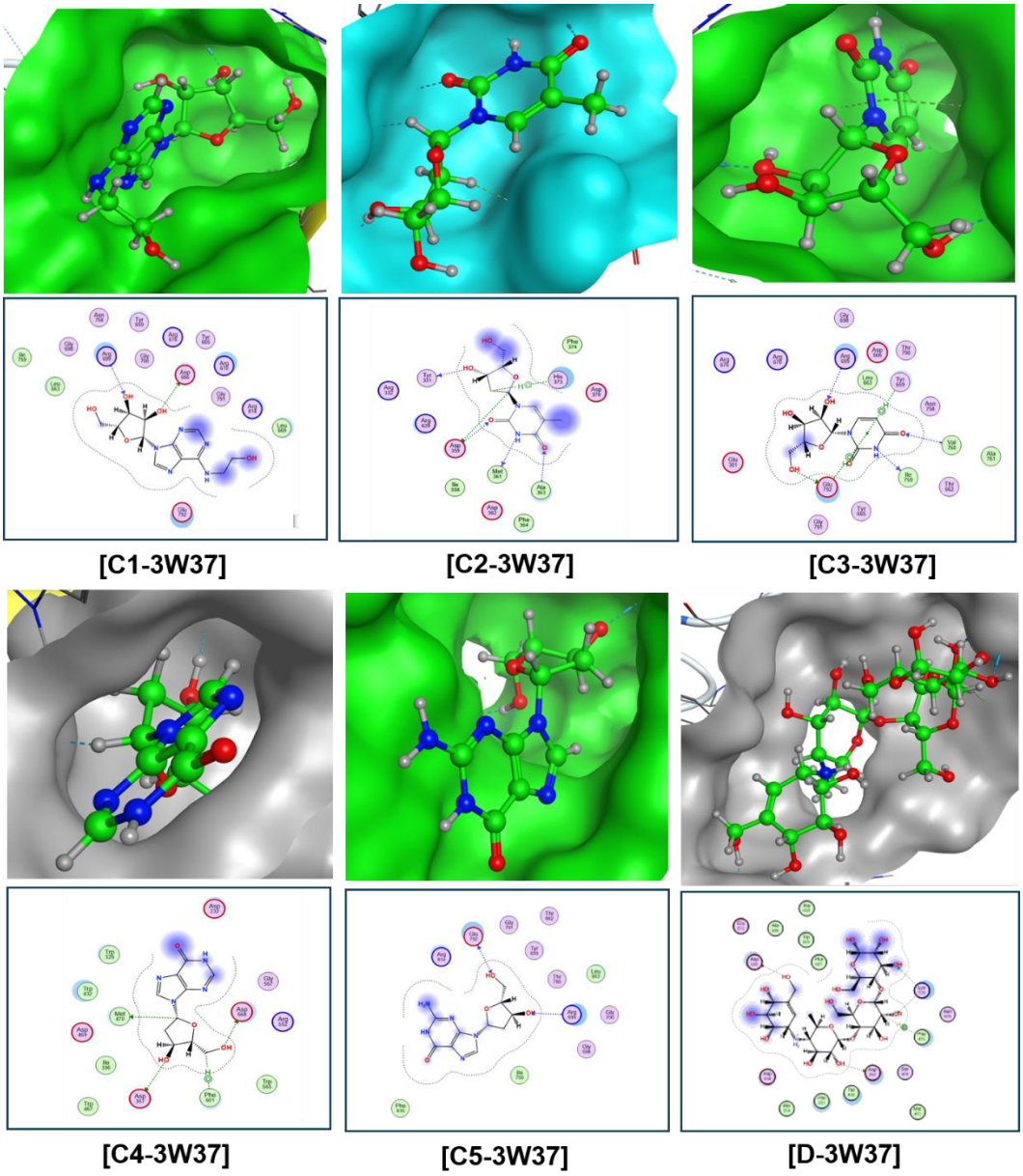


Figure 4. Visual presentation and in-pose interaction map of ligand-**3W37** (ligand: **C1–C5** and **D)** docking complex

3.3. Molecular dynamics simulation

Based on its favorable predicted binding affinity in molecular docking, **C3** was carried into a 100 ns MD simulation to test the stability of its complex with 3W37. The total energy (Figure 5A) plateaued between approximately -953000 and -940000 kJ.mol^{-1} without systematic drift, confirming the system reached equilibrium before analysis. The backbone RMSD (Figure 5B) of the **C3-3W37** complex fluctuated between approximately 0.10 and 0.37 nm over the first 60 ns before rising to ~0.65 nm at 60–80 ns, then stabilized near 0.28 nm for the remainder of the simulation. The RMSF analysis (Figure 5C) showed

that most backbone residues fluctuated within a low range of about 0.04 – 0.10 nm, supporting the overall stability of the **C3-3W37** complex; the few higher peaks (~0.20 – 0.33 nm) occurred in the flexible surface regions, mainly around residues 16 – 19 and 422 – 440, which are typical of solvent-exposed regions and away from the protein core.

SASA (Figure 5D) remained stable at ~310 – 314 nm^2, indicating limited change in solvent exposure over the simulation. Hydrogen bond (Figure 5E) analysis showed that three to four hydrogen bonds were preserved across most of the trajectory, with a drop to one or two between 60 and 80 ns followed by recovery, coinciding with the RMSD excursion over the same interval and indicating that the polar interactions break and reform rather than dissociating permanently. The Rg (Figure 5F) values were generally stable within 2.746 to 2.842 nm and showed no sustained drift or late stage expansion, indicating that the protein retained its compact fold throughout the simulation. These MD observations agree with the docking analysis: **C3** remained bound throughout the 100 ns trajectory with persistent interactions, supporting further experimental evaluation.

Taken together, Figures 5D, 5E and 5F show that C3 stayed inside the binding pocket at 60 – 80 ns. If the ligand had left, its hydrogen bonds to the protein would have fallen to zero, the emptied pocket would have raised SASA, and the protein would have swelled, increasing Rg. None of this occurred: one to two hydrogen bonds were kept throughout, SASA changed by only ~4 nm2, and Rg by less than 0.10 nm. The RMSD rise therefore reflects a temporary change in protein shape, not loss of the ligand.

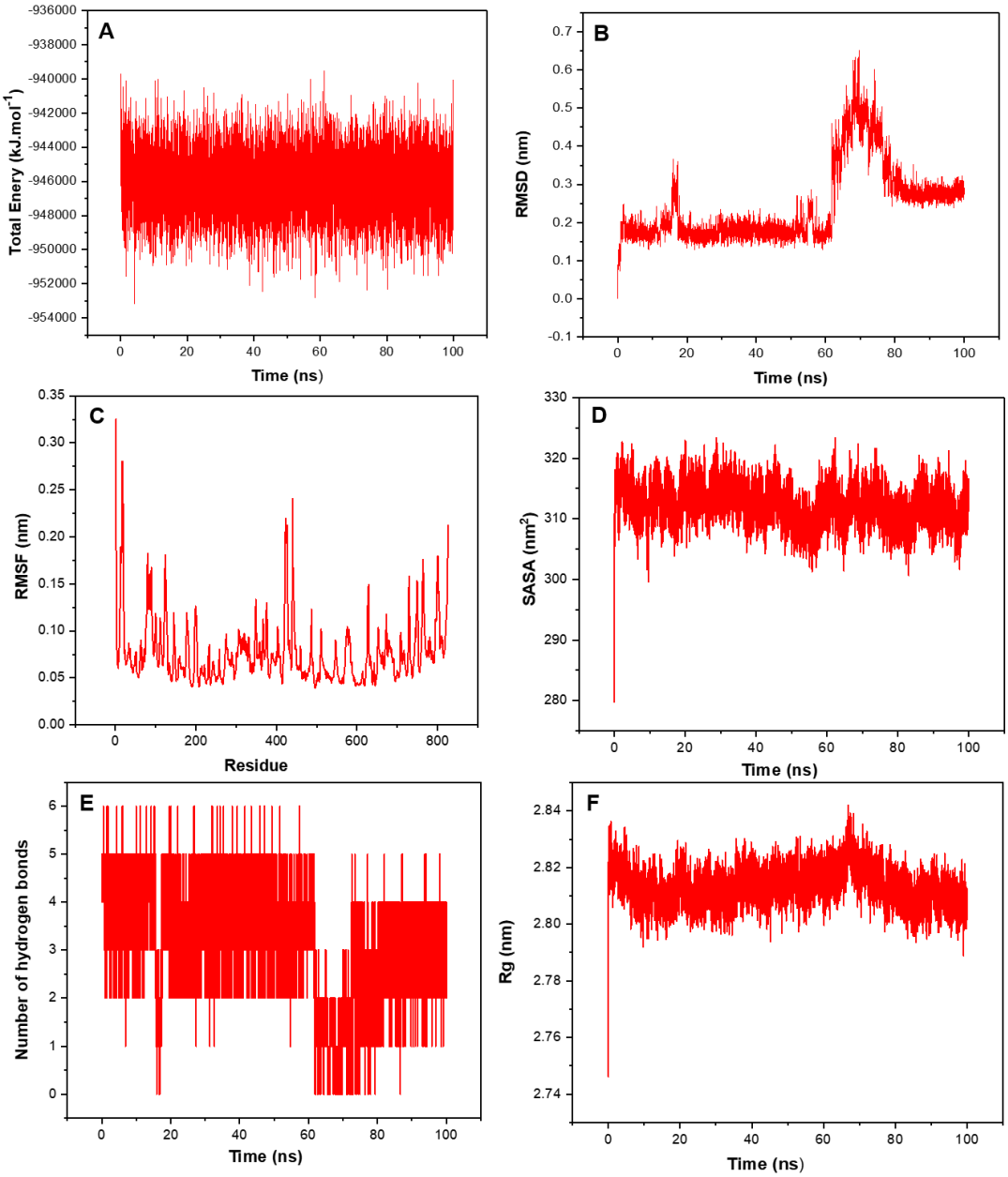


Figure 5. (A) Total energy, (B) RMSD, (C) RMSF, (D) SASA, (E) Hydrogen bonds and (F) Rg of the complex **[C3-3W37]**

3.4. Drug-likeness prediction

Table 5 summarizes the physicochemical parameters of the studied compounds **C1–C5.** The drug-likeness of **C1–C5** was assessed against Lipinski's Rule of Five (MW ≤ 500 Da, logP < 5, HBD ≤ 5, HBA ≤ 10), and all five compounds satisfied every criterion. Molecular weights fell between 242.09 Da (**C2**) and 311.12 Da (**C1**); logP values were negative throughout (-1.794 to -0.923), consistent with the polar character of nucleosides;

and donor/acceptor counts ranged from 3 to 5 and from 7 to 10, respectively (**C1**, 5/10; **C2**, 3/7; **C3**, 4/8; **C4**, 3/8; **C5**, 5/9). Molecular volumes spanned 213.933 Å^3 (**C3**) to 278.828 Å^3 (C1), and static polarizability 20.84 Å^3 (**C3**) to 29.14 Å^3 (**C1**), tracking the same rank order as volume. This compliance profile, together with the moderate molecular volumes and balanced donor/acceptor ratios, supported further evaluation of **C1–C5** as candidate α-glucosidase inhibitors, pending experimental validation. Ligand–protein interaction counts at 3W37 ranged from 2 to 6; **C3**, the smallest-volume compound with a balanced HBD/HBA ratio, reached the upper end of this range, suggesting that its compact framework allowed closer approach to a greater number of surrounding residues.

Table 5. Physicochemical properties of studied compounds

Ligand	Volume (Å^3)	Mass (Da)	Polarisability (Å^3)	LogS	LogP	HBD	HBA	Ligand-protein interactions
C1	278.828	311.12	29.14	-1.508	-1.143	5	10	2
C2	222.439	242.09	21.94	-0.708	-0.923	3	7	6
C3	213.933	244.07	20.84	-0.295	-1.794	4	8	6
C4	224.449	252.09	23.53	-1.615	-1.446	3	8	4
C5	235.446	267.1	24.70	-2.133	-1.353	5	9	3

3.5. ADMET prediction

To complement the docking and MD simulation results, ADMET properties of **C1–C5** were predicted and compared with acarbose (**D**) (Table 6). In terms of absorption, Caco-2 permeability across the series (-0.097 to 0.066 log Papp) was substantially higher than acarbose (-10.051 log Papp), and intestinal absorption was moderate for all five compounds (44.5–67.3%); C1 and C4 were predicted as P-glycoprotein substrates, while C3 was not, suggesting no predicted efflux-mediated barrier to oral delivery. Regarding distribution, BBB and CNS permeability values were negative throughout the series, consistent with limited central penetration and appropriate for a gastrointestinal peripheral target; **C3** had the most negative CNS permeability among the five (-5.338 log PS). In metabolism, no compound was predicted to interact with CYP2D6, CYP3A4, CYP1A2, CYP2C19, or CYP2C9 as a substrate or inhibitor, suggesting a low potential for CYP-mediated drug–drug interactions across the series. For excretion, total clearance was low and comparable across **C1–C5** (0.786–0.872 log mL.min^{-1}.kg^{-1}), markedly lower than acarbose (7.490 log mL.min^{-1}.kg^{-1}), and no compound was predicted as a renal OCT2 substrate, indicating passive glomerular filtration as the likely elimination route. Concerning toxicity, **C1** and **C4** were flagged for both Ames mutagenicity and hepatotoxicity, C5 for hepatotoxicity alone, while **C2** and **C3** were negative for both; no

compound inhibited hERG I or II channels. Among the five compounds, **C3** showed the most balanced ADMET profile: it carried no mutagenicity or hepatotoxicity flags and was not a P-glycoprotein substrate. Its predicted safety margins were also the most favorable in the series, with the highest maximum tolerated dose (1.711 log $mg.kg^{-1}.day^{-1}$), oral acute LD50 (2.78 $mol.kg^{-1}$), and chronic LOAEL (3.603 log $mg.kg^{-1}.day^{-1}$). These findings are consistent with the binding affinity and structural stability observed in docking and MD analyses, supporting **C3** as the primary candidate for further experimental investigation. All values are in silico predictions and require experimental confirmation.

Table 6. Pharmacokinetic and pharmacological properties of compounds **C1–C5** and **D** via ADMET analysis

Property	C1	C2	C3	C4	C5	D	Unit
Absorption							
Water solubility	-1.65	-1.8	-1.513	-1.647	-2.999	-2.892	(1)
Caco2 permeability	0.066	-0.009	-0.097	-0.003	-0.033	-10.051	(2)
Intestinal absorption (human)	48.418	60.32	44.51	67.25	65.304	100	(3)
Skin Permeability	-2.735	-2.884	-2.765	-2.735	-2.735	-2.735	(4)
P-glycoprotein substrate	Yes	No	No	Yes	No	No	(5)
P-glycoprotein I inhibitor	No	No	No	No	No	No	(5)
P-glycoprotein II inhibitor	No	No	No	No	No	No	(5)
Distribution							
VDss (human)	-0.562	-0.747	-0.802	-0.159	0.359	0.011	(6)
Fraction unbound (human)	0.743	0.667	0.637	0.677	0.787	0.381	(6)
BBB permeability	-1.807	-0.941	-1.272	-1.131	-1.506	-5.918	(7)
CNS permeability	-4.285	-4.432	-5.338	-3.459	-4.185	-7.532	(8)
Metabolism							
CYP2D6 substrate	No	No	No	No	No	No	(5)
CYP3A4 substrate	No	No	No	No	No	No	(5)
CYP1A2 inhibitor	No	No	No	No	No	No	(5)
CYP2C19 inhibitor	No	No	No	No	No	No	(5)
CYP2C9 inhibitor	No	No	No	No	No	No	(5)

CYP2D6 inhibitor	No	No	No	No	No	No	(5)
CYP3A4 inhibitor	No	No	No	No	No	No	(5)
Excretion							
Total Clearance	0.872	0.786	0.815	0.842	0.837	7.49	(9)
Renal OCT2 substrate	No	No	No	No	No	No	(5)
Toxicity							
AMES toxicity	Yes	No	No	Yes	No	Yes	(5)
Max. tolerated dose (human)	0.347	1.315	1.711	0.779	0.596	0.438	(10)
hERG I inhibitor	No	No	No	No	No	No	(5)
hERG II inhibitor	No	No	No	No	No	No	(5)
Oral Rat Acute Toxicity (LD50)	1.806	2.317	2.78	2.055	2.248	2.482	(11)
Oral Rat Chronic Toxicity (LOAEL)	2.942	2.675	3.603	1.996	2.193	11.386	(12)
Hepatotoxicity	Yes	No	No	Yes	Yes	No	(5)
Skin Sensitisation	No	No	No	No	No	No	(5)
T.Pyriformis toxicity	0.285	0.263	0.285	0.285	0.285	0.285	(13)
Minnow toxicity	3.807	3.562	3.948	3.346	3.853	-1.367	(14)

(1) log $mol.L^{-1}$; (2) log Papp (10^{-6} $cm.s^{-1}$); (3) %; (4) log Kp; (5) Yes/No; (6) log $L.kg^{-1}$; (7) log BB; (8) log PS; (9) log $mL.min^{-1}.kg^{-1}$; (10) log $mg.kg^{-1}.day^{-1}$; (11) $mol.kg^{-1}$; (12) log $mg.kg^{-1}_bw.day^{-1}$; (13) log $\mu g.L^{-1}$; (14) log mM

4. CONCLUSION

The five *C. cicadae* nucleosides were screened against α-glucosidase (3W37) by docking, MD simulation, drug-likeness assessment, and ADMET prediction. Binding-site prescreening favored Site 2 for **C1**, **C3**, and **C5**, Site 1 for **C4** and **D**, and Site 4 for **C2**. Docking scores ranked **C3** (-12.0 $kcal.mol^{-1}$) > **C2** (-11.9 $kcal.mol^{-1}$) > C4 (-11.6 $kcal.mol^{-1}$) > **C5** (-10.8 $kcal.mol^{-1}$) > **C1** (-10.0 $kcal.mol^{-1}$), comparable to acarbose (**D**, -12.1 $kcal.mol^{-1}$); **C3**, with the lowest docking score energy (DS), was selected for further study. Over 100 ns, the **C3-3W37** complex remained stable: RMSD stabilized near 0.28 nm after a transient shift at 60 – 80 ns, RMSF stayed within 0.04-0.10 nm for most residues, Rg held within 2.746 – 2.842 nm, SASA remained near a baseline of ~310–314 nm^2, and three to four hydrogen bonds persisted for most of the trajectory. All five compounds satisfied Lipinski's Rule of Five, with ADMET profiling indicating generally favorable

pharmacokinetic and safety profiles across the series and **C3** showing the most favorable overall margin. These *in silico* findings support C3 as a promising α-glucosidase inhibitor candidate that deserves further experimental study

ACKNOWLEDGEMENT

This study is a result of the municipal-level Science and Technology project funded by the Hue City state budget (Project Code: THH.2023-KC.04).

REFERENCES

[1]. K. S. Polonsky, and C. F. Burant (2015). Type 2 Diabetes Mellitus, Williams Textb. Endocrinol., Vol. 1, no. 1, pp. 1385–1450.

[2]. M. Alssema, C. Ruijgrok, E. E. Blaak, L. Egli, P. Dussort, S. Vinoy, J. M. Dekker, and M. Denise Robertson (2021). Effects of alpha-glucosidase-inhibiting drugs on acute postprandial glucose and insulin responses: a systematic review and meta-analysis, Nutr. Diabetes, Vol. 11, no. 1, p. 11.

[3]. U. Ghani (2015). Re-exploring promising α-glucosidase inhibitors for potential development into oral anti-diabetic drugs: Finding needle in the haystack, Eur. J. Med. Chem., Vol. 103, pp. 133–162.

[4]. G. Das, H. S. Shin, G. Leyva-Gómez, M. L. D. Prado-Audelo, H. Cortes, Y. D. Singh, M. K. Panda, A. P. Mishra, M. Nigam, S. Saklani, P. K. Chaturi, M. Martorell, N. Cruz-Martins, V. Sharma, N. Garg, R. Sharma, and J. K. Patra (2021). Cordyceps spp.: A Review on Its Immune-Stimulatory and Other Biological Potentials, Front. Pharmacol., Vol. 11, p. 602364.

[5]. O. J. Olatunji, J. Tang, A. Tola, F. Auberon, O. Oluwaniyi, and Z. Ouyang (2018). The genus Cordyceps: An extensive review of its traditional uses, phytochemistry and pharmacology, Fitoterapia, Vol. 129, pp. 293–316.

[6]. S. A. Ashraf, A. E. O. Elkhalifa, A. J. Siddiqui, M. Patel, A. M. Awadelkareem, M. Snoussi, M. S. Ashraf, M. Adnan, and S. Hadi (2020). Cordycepin for Health and Wellbeing: A Potent Bioactive Metabolite of an Entomopathogenic Medicinal Fungus Cordyceps with Its Nutraceutical and Therapeutic Potential, Molecules, Vol. 25, no. 12, p. 2735.

[7]. J. Wang, Z. Zhang, Y. Wang, M. Yang, C. Wang, X. Li, and Y. Guo (2017). Chemical Constituents from Mycelia and Spores of Fungus Cordyceps cicadae, Chinese Herb. Med., Vol. 9, no. 2, pp. 188–192.

[8]. Z. B. Chu, J. Chang, Y. Zhu, and X. Sun (2015). Chemical constituents of cordyceps cicadae, Nat. Prod. Commun., Vol. 10, no. 12, pp. 2145–2146.

[9]. Chemical Computing Group ULC (2024). Molecular Operating Environment (MOE). Version 2022.10 [Software]. Montreal, QC, Canada.

[10]. B. Hess, H. Bekker, H. J. C. Berendsen, and J. G. E. M. Fraaije (1997). LINCS: A Linear Constraint Solver for molecular simulations, J. Comput. Chem., Vol. 18, no. 12, pp. 1463–1472.

[11]. C. A. Lipinski, F. Lombardo, B. W. Dominy, and P. J. Feeney (2001). Experimental and computational approaches to estimate solubility and permeability in drug discovery and development settings, Adv. Drug Deliv. Rev., Vol. 46, no. 1–3, pp. 3–26.

[12]. D. E. V. Pires, T. L. Blundell, and D. B. Ascher (2015). pkCSM: Predicting small-molecule pharmacokinetic and toxicity properties using graph-based signatures, J. Med. Chem., Vol. 58, no. 9, pp. 4066–4072.

[13]. T. Tagami, K. Yamashita, M. Okuyama, H. Mori, M. Yao, and A. Kimura (2013). Molecular basis for the recognition of long-chain substrates by plant α-glucosidases, J. Biol. Chem., Vol. 288, no. 26, pp. 19296–19303.

[14]. T. T. Phuong Thao, T. Q. Bui, P. T. Quy, N. C. Bao, T. Van Loc, T. Van Chien, N. L. Chi, N. Van Tuan, T. Van Sung, and N. T. Ai Nhung (2021). Isolation, semi-synthesis, docking-based prediction, and bioassay-based activity ofDolichandrone spathaceairidoids: new catalpol derivatives as glucosidase inhibitors, RSC Adv., Vol. 11, no. 20, pp. 11959–11975.

SÀNG LỌC *IN SILICO* CÁC NUCLEOSIDE TỪ *CORDYCEPS CICADAE* LÀM CHẤT ỨC CHẾ α-GLUCOSIDASE TRONG ĐIỀU TRỊ ĐÁI THÁO ĐƯỜNG

Nguyễn Công Kính[1,2], Nguyễn Đại Châu[1], Phạm Văn Vinh[1], Nguyễn Vĩnh Phú[3], Phan Tứ Quý[4], Trần Quang Huy[1], Nguyễn Thị Thanh Hải[1], Nguyễn Thị Ái Nhung[1,*]

[1]Khoa Hóa học, Trường Đại học Khoa học, Đại học Huế

[2] Khoa Dược, Đại học Duy Tân

[3]Khoa Cơ bản, Trường Đại học Y – Dược, Đại học Huế

[4]Khoa Khoa học Tự nhiên, Trường Đại học Tây Nguyên

*Email: ntanhung@hueuni.edu.vn

TÓM TẮT

Ức chế α-glucosidase làm chậm tiêu hóa carbohydrate ở ruột là chiến lược thực tiễn để kiểm soát tăng đường huyết sau ăn trong đái tháo đường. Năm nucleoside và dẫn xuất nucleoside được lựa chọn từ *Cordyceps cicadae* gồm N6-(2-hydroxyethyl)-adenosine (**C1**), thymidine (**C2**), uridine (**C3**), 2′-deoxyinosine (**C4)** và 2′-deoxyguanosine (**C5**) được đánh giá có khả năng ức chế α-glucosidase (PDB ID: 3W37) bằng mô phỏng lắp ghép phân tử, mô phỏng động lực học phân tử, đánh giá hoạt tính "giống thuốc" và dự đoán ADMET, với acarbose làm đối chứng (**D**). Sàng lọc sơ bộ trên bốn vị trí tiềm năng của protein 3W37 để xác định vị trí docking tối ưu cho từng hợp chất, cho thấy khả năng ức chế protein 3W37 của phối tử **C1 – C5** thông qua năng lượng liên kết dự đoán được sắp xếp giảm dần: **C3** (-12,0 kcal.mol^{-1}) > **C2** (-11,9 kcal.mol^{-1}) > **C4** (-11,6 kcal.mol^{-1}) > **C5** (-10,8 kcal.mol^{-1}) > **C1** (-10,0 kcal.mol^{-1}). Trong đó **C3** gắn kết dự đoán thuận lợi nhất cùng 12 tương tác van der Waals tại Vị trí 2. Chỉ số RMSD của phức **C3-3W37** ổn định trở lại quanh 0,28 nm sau dao động nhẹ ở 60 – 80 ns; trong giai đoạn này, số lượng liên kết hydrogen giảm từ mức 3 – 4 liên kết xuống còn 1 – 2 liên kết, trong khi giá trị Rg và SASA vẫn duy trì ổn định. Các hợp chất nghiên cứu đều thỏa mãn Quy tắc 5 của Lipinski, và phân tích ADMET cho thấy đặc tính dược động học thuận lợi, trong đó **C3** có mức an toàn được dự đoán phù hợp. Trong phạm vi nghiên cứu in silico, **C3** được xác định là ứng viên tiềm năng cho nghiên cứu thực nghiệm ức chế α-glucosidase.

Từ khóa: *Cordyceps cicadae*, α-glucosidase, 3W37, nghiên cứu tính toán.